

Predict-and-Update Network: Audio-Visual Speech Recognition Inspired by Human Speech Perception

Jiadong Wang, Xinyuan Qian, *Member, IEEE*, Haizhou Li, *Fellow, IEEE*,

Abstract—Audio and visual signals complement each other in human speech perception, so do they in speech recognition. The visual hint is less evident than the acoustic hint, but more robust in a complex acoustic environment, as far as speech perception is concerned. It remains a challenge how we effectively exploit the interaction between audio and visual signals for automatic speech recognition. There have been studies to exploit visual signals as *redundant* or *complementary* information to audio input in a synchronous manner. Human studies suggest that visual signal primes the listener in advance as to when and on which frequency to attend to. We propose a Predict-and-Update Network (P&U net), to simulate such a visual cueing mechanism for Audio-Visual Speech Recognition (AVSR). In particular, we first predict the character posteriors of the spoken words, i.e. the visual embedding, based on the visual signals. The audio signal is then conditioned on the visual embedding via a novel cross-modal Conformer, that updates the character posteriors. We validate the effectiveness of the visual cueing mechanism through extensive experiments. The proposed P&U net outperforms the state-of-the-art AVSR methods on both LRS2-BBC and LRS3-BBC datasets, with the relative reduced Word Error Rate (WER)s exceeding 10% and 40% under clean and noisy conditions, respectively.

Index Terms—predict-and-update, audio-visual speech recognition, early fusion

I. INTRODUCTION

HUMANS have developed five senses: smell, taste, balance, vision, and hearing as a result of evolution. Among these senses, vision and hearing are primarily involved during social interaction and for effective perception. Human speech perception benefits from combining audio and visual modalities with their unique and complementary characteristics.

It is apparent that multi-modal solutions, *e.g.*, audio and visual, outperform their unimodal counterparts in speech processing tasks such as speech extraction [1], active speaker detection [2], and emotion recognition [3]. Automatic Speech Recognition (ASR) performance deteriorates in the presence of acoustic noise [4], [5], and so does human speech recognition: the pair of /m/ and /n/, /b/ and /d/ are acoustically less distinguishable under noise [6]. Visual signals become very useful in a noisy environment because they are not affected by acoustic noise. One of the challenges is that many-to-one phoneme-to-viseme mapping exists [7]. In other words, multiple phonemes (up to 13) could be rendered with the same lip movement [7]. The question is how to effectively make use of such an inexact visual cue in speech recognition.

In a human speech perception study [8], Summerfield made three hypotheses about the possible roles of video modality in improving noisy speech intelligibility. 1) Lipreading offers segmental and suprasegmental hints *redundant* to audio hints. In other words, the phonetic information of speech is



Fig. 1. The universal diagram of end-to-end lip reading or ASR. Input can be video or audio.

equally available in both audio and video modalities. For example, consonants and vowels are segmental, while rhythm, stress, and intonation are suprasegmental. 2) Lipreading offers segmental and suprasegmental hints *complementary* to audio hints. That is, visual hints provide information unavailable in audio hints, perhaps due to acoustic interference. 3) When one listens, the audio signals (attended speech) and the video signals (lip movements) share common spatial-temporal properties, which may guide listeners to focus on speech signals of interest rather than acoustic interference.

The studies of the first two hypotheses in human speech perception serve as the motivations for implementing of AVSR. As audio and visual signals are *redundant* or *complementary*, they can be fused at the decision level or feature level for improved robustness. At the decision level, we may fuse the decisions made by individual modalities through weighted summation [9], [10] or network [11]. At the feature level, the fusion of either raw features or context representations was studied. A straightforward solution is to first combine raw audio and visual features via concatenation [12], [13], [14] and then apply sequence modeling and decoding. On the other hand, we may first encode the context representations of audio and visual signals from the short-time (raw) features, then fuse them, for example, by concatenation with audio-visual alignment [15], [16] or without [17].

In the third hypothesis, a visual cueing mechanism is suggested: lip movement preceding voice [18] can influence hearing at an elementary level, cueing listeners when and on which frequency of speeches one should focus [19], [20]. As well known, plosives consist of closure and release in order where only the latter is audible while both are visible [21]. Thus, visible closure may help predict the coming voice [18]. In a psycho-acoustic experiment, human subjects attempted to distinguish 10 different French syllables pronounced with similar lip movements [22]. Lips were found to move before the arrival of the voice, which prompts listeners to pay attention to sounds, resulting in improved intelligibility. A similar visual cueing effect was reported in the experiment on bird song identification [23]. It was shown that if humans know when a bird song is playing, they can better identify the

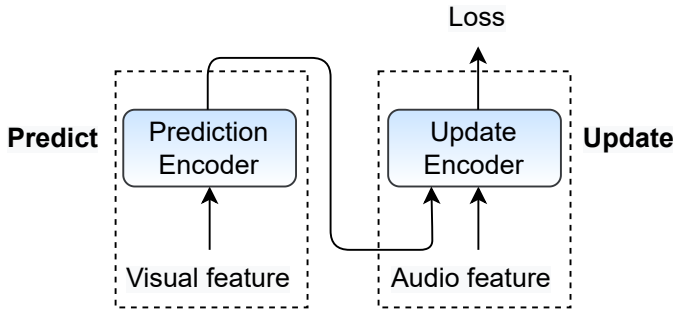


Fig. 2. The general block diagram of our proposed P&U net which adopts video modality to predict a sequence of a coarse probability distribution, *i.e.*, visual embedding, towards the target text transcription. The audio input is then augmented with the visual embedding for speech recognition via an update encoder.

specific bird to which the bird song belongs in the acoustic interference without any additional cue, such as a spatial cue. In this case, the simple indication of the onset and offset of the target song in the interference benefits human perception.

Furthermore, in the study of the video modality that helps human speech detection, the high similarity between lip-opening area functions and acoustic envelope bands ($F2$, $F3$) is found [19] with up to 165 ms of audio lag, which shows the potential of video to reduce temporal and frequency uncertainty. Further experiments about human speech detection demonstrate that, with video, results of $F2$ -filtered speeches by bandpass are comparable to those of unfiltered speeches, while those of $F1$ -filtered speeches are not comparable [20]. Therefore, preceding the corresponding voice, video modality cues listeners to focus when in time and at which frequency on the spectrum.

We are motivated to implement the mechanism in the third hypothesis in a neural architecture. The question is how to effectively benefit from the visual cue with computational efficiency. We propose to use the prediction of spoken characters from the visual signal as the visual cue. In view of the fact that video modality is ambiguous but noise-invariant while audio modality is explicit but noise-vulnerable, we adopt a predict-and-update network architecture, where particle filter [24], [25] and Kalman filter [25] are employed for a pair of sensory inputs in robotics, just like audio and visual signals.

The predict-and-update network, *i.e.*, the P&U net, emulates the visual cueing mechanism in human speech perception by considering the distinct characteristics of the audio and video modalities. As shown in Fig. 2, we first take visual input to predict the probability distributions of spoken text in terms of characters, which is called *visual embedding*. We then fuse the visual embedding with the audio features to update the probability distributions. The visual cueing mechanism in the update encoder can be implemented using a factorized-excitation Feed Forward Network (FFN) with the same parameter structure as vanilla FFN. Our contributions are summarized as follows:

- 1) We propose a P&U net to emulate the visual cueing mechanism in human speech perception while considering the heterogeneous characteristics of audio and visual

signals.

- 2) We design a factorized-excitation FFN for audio sequence modelling that effectively benefits from the visual cues.
- 3) The proposed audio-visual speech recognition network outperforms other state-of-the-art AVSR methods [17] by a large margin, especially in a noisy environment.

II. RELATED WORK

We start by reviewing how audio-visual fusion is implemented in the literature to set the stage for this work. The studies of the first two hypotheses in human speech perception have motivated many audio-visual fusion implementations. In particular, audio and visual signals are considered redundant, complementary, and synchronous.

With decision-level fusion, we make the final decisions by combining the decisions of individual modalities [9], [10], [26], where audio-visual alignment information is not fully exploited. For instance, one can multiply the audio and visual decision probabilities to make a final decision [6]. Note that audio and video modality have own unique properties, their contributions should be considered separately. In [9], reliability is implemented in making the final decision by weighting between the audio (0.7) and visual (0.3) modality, as audio is more representative in a clean environment. To account for a varying environment, dynamic weights of audio and video modality are applied in [10], [27]. In [27], dynamic weights are controlled by a logistic function of estimated Signal-to-noise ratio (SNR). Recently, decision probabilities are fused with their quality indicators of audio and video modalities (*i.e.*, SNR for audio and facial action unit for video), for example, by a Long Short-Term Memory (LSTM) or fully-connected layer. The decision-level fusion techniques mostly combine text posteriors from two modalities for speech recognition. They follow the idea that audio-visual information is *redundant* or *complementary*. However, they do not explicitly use synchronization or interaction between audio and video [28].

It is also straightforward to fuse audio and visual signals at the feature level. Fusion can take place between raw features [12], [13], context representations [4], [29], [30], or a mix of both [31], [32]. The fusion of context representations is widely used by concatenation [4], [29] or multiplication [30]. The feature fusion techniques seek to make use of the synchronization information. Some looked into audio-visual alignment before the feature concatenation by varying the hop size of short-time Fourier transform (STFT) [13] or resampling visual signals to the rate of the audio spectrum [12]. Others studied the audio-visual interaction by cross-modal attention, where audio context representation is used to query visual context representation to generate audio-aligned visual representation [15], [33]. This mechanism offers a temporally aligned visual representation to the audio representation. Similarly, visual context representation can also be used to query audio context representation [16] to fully use the audio-visual interaction. There was also an attempt [34] to map audio and visual raw features to a shared representation to normalize the inherent

different modalities. In general, feature-level fusion techniques seek to exploit the audio-visual synchronization property. They have not exploited the asynchronization between audio and visual signals at the time of feature fusion, where the visual signal is processed ahead of the audio signal.

In general, all fusion studies are motivated by the belief that audio and visual signals are redundant and complementary in a synchronous manner. They have not made use of the audio-visual interaction as discovered in the third hypothesis [8] by Summerfield. We are motivated to explore such audio-visual interaction in this work.

III. PREDICT-AND-UPDATE NETWORK

We now propose a novel neural architecture, P&U net, for AVSR, as shown in Fig. 3. In particular, we will elaborate on how the predict-and-update framework emulates the human visual cueing mechanism.

A. Audio and visual features

Spectral features are widely used as acoustic features for speech signals in speech recognition [4], [16]. We adopt Short-time Fourier transform (STFT) as the spectral feature, as in other AVSR studies [4], [35]. To compute the spectral features, we adopt a window size of 40 ms and a window shift of 10 ms that converts a speech utterance into a sequence of 321-dimensional speech frames. Subsequently, a Convolutional Neural Network (CNN) module is adopted to down-sample one in four frames so that the frame rate of speech features is aligned with that of the video frame sequence at 25 Frames per Second (FPS).

The visual signal is sampled at 25 FPS. We crop a 122×122 patch from each 224×224 image for pre-processing. We adopt ResNet [36] to generate visual features considering both performance and training effort [36]. Therefore, we apply a 3D convolutional layer followed by a 2D ResNet-18 [36] on image sequences as the visual extractor. The kernel size of the 3D convolutional layer is $5 \times 7 \times 7$ (time, height, width). After ResNet-18, we employ a global average pooling layer to reach the expected feature dimensions.

B. Prediction

We design a predictor to generate a contextual representation, *i.e.*, visual embedding, from a video sequence. The predictor predicts the arrival of sound ahead of time. To this end, an encoder is required to encode the temporal information from a video sequence. There are many options for encoders, such as LSTM [15], [37], Gated Recurrent Unit (GRU) [35], [38], and Transformer [4], [39]. Despite great success, it was argued that these encoders have not explicitly leveraged short-range temporal dependencies [40]. The fully-CNN encoder is one of the solutions for ASR [41] and lip-reading [42]. Recently, Conformer [17], [43] has shown outstanding performance taking advantage of both CNN and the transformer, which are good at modelling local and global dependencies [17]. We therefore adopt Conformer as our encoders.

As shown in Fig. 3(c)-Fig. 3(d), the prediction network consists of some stacked Conformer blocks [43] and a projection head. The Conformer blocks model temporal dependency in the visual sequence, while the projection head compresses the visual representation to a low-dimension character posterior with a softmax function. As shown in Fig. 1, a Conformer block consists of a FFN layer, a Multi-Head Self Attention (MHSA) module, a convolutional block, and another FFN layer in a pipeline. A layer normalization module is applied before each sub-module in the Conformer block.

The MHSA module takes as input the query $Q \in \mathbb{R}^{T \times d_k}$, key $K \in \mathbb{R}^{T \times d_k}$ and value $V \in \mathbb{R}^{T \times d_k}$ with relative positional encoding, where T is the number of frames in an utterance and d_k is the dimension of query, key, and value. The MHSA module first maps the set of three inputs to h sets according to h heads and then calculates the scaled dot-product attention which is depicted in [39]. The convolutional block consists of two pointwise 1D convolutional layers and a depthwise 1D convolutional layer with a skip connection. It outputs a hidden audio feature $\zeta^c \in \mathbb{R}^{T \times d_a}$, where d_a is the feature dimension. By combining the convolutional block and the self-attention module [39], the Conformer as an encoder is capable of modeling both local and global interactions of visual features. The FFN process is formulated as:

$$FFN(\tau) = W_2 \times \phi(W_1 \tau^\top + B_1) + B_2 \quad (1)$$

where $\tau \in \mathbb{R}^{T \times d_a}$ is the input. $W_1 \in \mathbb{R}^{d_{ff} \times d_a}$, $B_1 \in \mathbb{R}^{d_{ff}}$ and $W_2 \in \mathbb{R}^{d_a \times d_{ff}}$, $B_2 \in \mathbb{R}^{d_a}$ are the parameters of the first and second linear layers. ϕ is an activation function. In short, FFN firstly transforms τ from d_a -dimensions to d_{ff} -dimensions and then transforms it back to d_a -dimensions.

Finally, the projection head generates the visual embedding $\rho \in \mathbb{R}^{T \times C}$, which is a sequence of T frames. Each frame is represented by a C -dimension character posterior. The prediction module can be pre-trained on a lipreading task, which aligns ρ with the target character by CTC and attention decoder loss to ensure that the predictor outputs are phonetically relevant to the output text. The training loss will be discussed in Sec. III-D.

C. Update

We design an update encoder in Fig. 3(c) to produce an audio-visual context representation from the visual embedding and the raw audio feature. This encoder emulates the visual cueing mechanism. Then the audio-visual context representation is passed to the decoder and the CTC module.

In the update encoder, the audio-visual fusion is achieved by stacking N_{cc} cross-modal Conformer blocks. In different cross-modal Conformer blocks, the visual embedding joins the hierarchical audio features, as the visual embedding in the form of character posteriors is closer to the output text than the hierarchical audio features in shallow blocks. This fusion emulates the visual-cueing mechanism. Visual-cued audio features are then processed by N_c vanilla Conformer blocks, that generate audio-visual contextual representation, *i.e.*, the updated text posteriors.

The cross-modal Conformer block is a revised version of the vanilla configuration [43] by replacing the original FFN

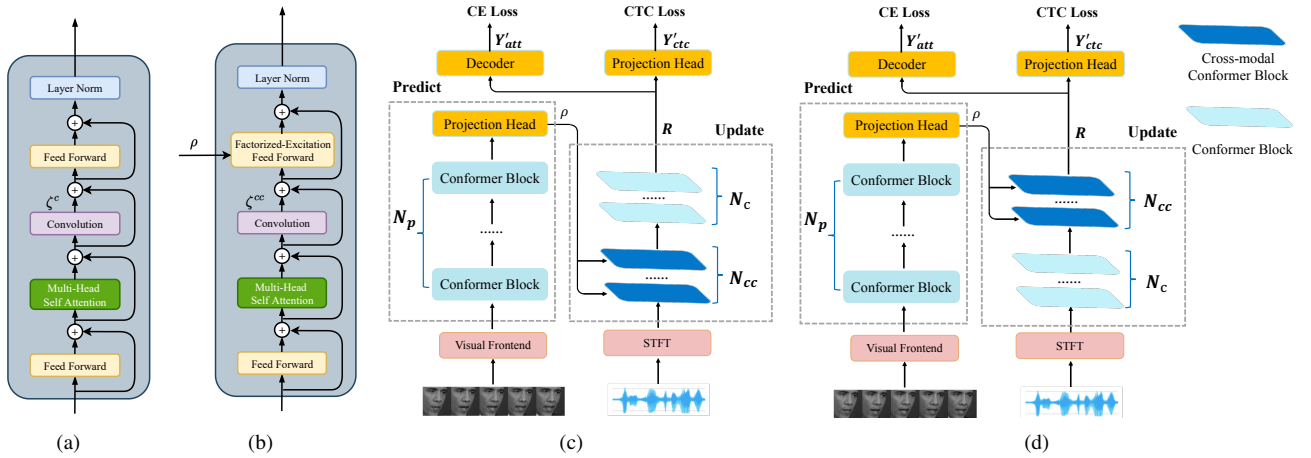


Fig. 3. Neural architecture of the predict-and-update network: a) Conformer block; b) Cross-modal conformer block. ρ denotes visual embedding from visual input; ζ^c and ζ^{cc} are the outputs of the convolutional blocks in the Conformer and the cross-modal Conformer, respectively and c) our proposed P&U net (early) where the audio input is conditioned on the visual embedding at an early stage, d) a contrastive architecture of P&U net (late) where the audio input is conditioned on a late stage. Notes: N_p is the number of the Conformer blocks in the prediction encoder; N_c and N_{cc} are the number of the Conformer and the cross-modal Conformer block in the update encoder. Y'_{att} and Y'_{ctc} are hypotheses about text sequence for CE loss and CTC loss, respectively. R is the audio-visual context representation.

[39] after the convolutional block with a proposed factorized-excitation FFN, as illustrated in Fig. 4. We also propose a contrastive architecture by swapping the Conformer and the cross-modal Conformer blocks, as illustrated in Fig. 3(d), to observe the effect between early fusion and late fusion.

The factorized-excitation FFN is inspired by the factorized layer, which has been implemented in ASR [44] and speech extraction [45]. It is typically used to condition the network on prior external knowledge. Thus, it is a perfect mechanism to take visual cues to strengthen speech encoding. In [44], the factorized layer is used to adapt the ASR model to acoustic conditions with varying speaker genders, identities and noise SNR, where the results of different conditions are summed with external factors. The factorized layer is formulated as:

$$X^{i+1} = \sum_{k=1}^K \alpha_k (\omega_k X^i + b_k) \quad (2)$$

where K is the number of subspaces that represents the conditions. X^i is an input of neurons in layer i and is mapped to different subspaces through ω_k and b_k . α_k are external factors and can be calculated by clustering [44]. In speech extraction [45], a reference from the target speaker's speech is used as a condition to guide speech extraction. Such a reference can be a fixed speaker embedding across time [46], or a frame-varying embedding sequence [47]. The previous studies suggest that the factorized layer is effective in conditioning the network on prior knowledge for speech processing.

Although the factorized layer effectively employs prior knowledge, which is the visual embedding herein, how to design a cross-modal Conformer block with the factorized layer is worthy of discussion [48]. We prefer a cross-modal Conformer block [43] that shares the same parameter architecture as the vanilla Conformer block in the ASR task, because

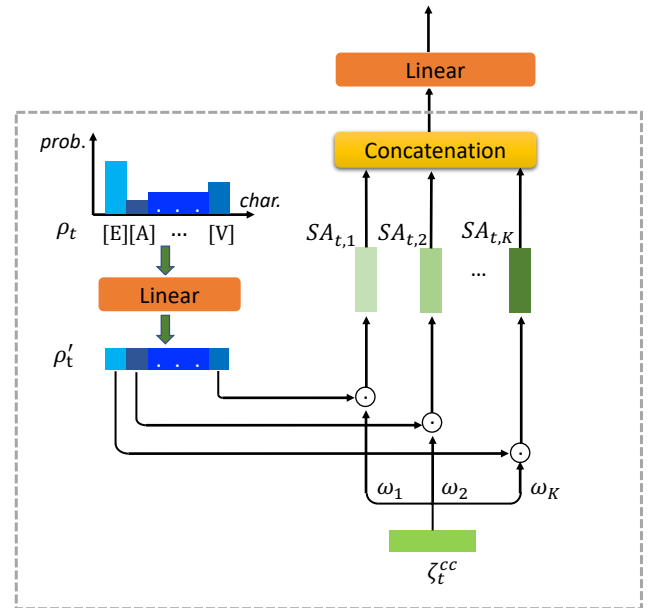


Fig. 4. The diagram of the factorized-excitation FFN module. An activation layer after the concatenation is omitted for brevity; ζ_t^{cc} and ρ_t denote the hidden audio features and the visual embedding from vision at frame t . $\omega_1 \dots \omega_K$ are shared across all time frames.

such a cross-modal Conformer block could potentially be pre-trained on an abundantly available audio-only dataset.

Therefore, we design a factorized-excitation FFN to modulate the audio features by conditioning on the visual embedding, and keep the same parameter architecture as the vanilla FFN.

The factorized-excitation FFN replaces the first linear layer of the vanilla FFN, as shown in the dotted grey box in Fig. 4, and keeps the second linear layer of the vanilla FFN. Therefore, we consider that the cross-modal Conformer

preserves the vanilla Conformer architecture. The dotted box processes the convolutional block’s output ζ^{cc} and the visual embedding ρ frame-by-frame as follows, where we take the t -th frame as an example.

$$\rho'_t = W_\rho \rho_t + B_\rho \quad (3)$$

where $\rho'_t \in \mathbb{R}^K$ is a variant of $\rho_t \in \mathbb{R}^C$, W_ρ and B_ρ are parameters of the linear layer.

$$SA_{t,k} = \rho'_{t,k} \omega_k \zeta_t^{cc} + b_k \quad (4)$$

where $SA_{t,k} \in \mathbb{R}^{d_l}$ denotes the k -th subspace; ζ_t^{cc} is the output of the convolutional block taken by the factorized-excitation FFN as the input, as shown in Fig. 3 and Fig. 4; We transform ζ_t^{cc} to $SA_{t,k}$ by applying $\omega_k \in \mathbb{R}^{d_l \times d_a}$ and $b_k \in \mathbb{R}^{d_l}$ with the prior knowledge $\rho'_{t,k}$. We make sure that $d_l \times K = d_{ff}$ so that the concatenation of all w_k has the same dimension as W_1 in Eq. 1. So do all b_k . Thus, \mathcal{F}_t has the same dimension as the output of the first linear layer of the vanilla FFN,

$$\mathcal{F}_t = \phi(\text{Concat}(SA_{t,1}, SA_{t,2}, \dots, SA_{t,K})) \quad (5)$$

where ϕ is an activation function.

With the factorized-excitation FFN, the update encoder benefits from both the pre-trained acoustic model and the visual embedding.

D. Loss function

We update the model parameters during training by gradient back-propagation subject to some loss functions. The model includes the mapping modules, the update encoder, the predictor, and the feature extractors. The mapping modules are used to predict text sequence from the audio-visual context representation.

An AVSR system [4], [49] may employ the CTC loss [50], to force monotonic alignment between the audio-visual context representation and the text sequence, where it is assumed that audio-visual frames are independent of one another [51]. The attention-based loss [52] represents another line of thought, which considers inter-frame dependency via an attention mechanism. However, the attention-based loss does not enforce monotonic alignment [29]. To benefit from the best of the two techniques, we adopt the hybrid CTC / attention method [53], [17] as the loss function of the P&U net, that delivers promising results [17].

Let us denote $Y \in \mathbb{R}^{L \times C}$ as the ground truth, *i.e.*, the text sequence and $R \in \mathbb{R}^{T \times d_a}$ as the audio-visual context representation, where L , T , d_a are the length of the text sequence, the number of frames of the audio-visual context representation, and the dimension of the update encoder of the audio-visual context representation, respectively.

In practice, the mapping module of the CTC loss is a linear layer followed by a softmax layer to get the posterior probabilities of C classes at all frames $Y'_{ctc} \in \mathbb{R}^{T \times C}$. Afterwards, dynamic programming is used to align the text sequence Y and posterior probabilities Y'_{ctc} .

The mapping module of the attention loss is a transformer decoder [39], [54] consisting of several transformer blocks. During training, the transformer decoder is adopted to parallelly predict all texts in an utterance from an audio-visual context representation R and a text sequence Y . All predicted texts form the text hypothesis Y'_{att} . The CE loss is applied to reduce the error between Y'_{att} and Y . During inference, the decoder generates characters one by one to form a character sequence. Unlike the Conformer, the transformer decoder uses absolute positional encoding.

Due to the hybrid training framework, the total loss function is formulated as the weighted sum of CTC loss and attention-based loss, formulated as:

$$\mathcal{L} = \lambda p_{ctc}(Y|R) + (1 - \lambda) p_{att}(Y|R) \quad (6)$$

where p_{ctc} and p_{att} are losses of CTC and attention, λ is the coefficient to control influences of two loss components.

E. Predict-and-Update vs. feature concatenation

The proposed predict-and-update strategy is different from feature concatenation in terms of the design concept and the actual implementation. First, with predict-and-update, we use visual signals to predict the character posterior that is phonetically informing. The fusion takes place between the phonetically informed output distributions and the raw audio features. However, in feature concatenation, the raw features of audio and visual signals are simply put together in the early stage without reference to a text or phonetic content. Second, the visual prediction is achieved through several Conformer blocks that effectively use a video sequence ahead of the arrival of audio sounds, similar to that in the visual cueing mechanism [22], to prime the listener when and on which frequency to focus.

IV. EXPERIMENT

In the visual cueing mechanism by humans, we observe two properties, 1) a preceding visual signal primes the listener what sounds are expected, 2) the expected sounds serve as the cue to the audio signal. The P&U net is designed to study the effect of the above two properties. We first design experiments where the visual embedding primes the update encoder at different stages of audio sequence modelling, *i.e.*, early cueing vs. late cueing. We then compare the proposed methods with some State-of-the-Art (SOTA) systems. As a contrastive system, we also evaluate the traditional feature concatenation technique in comparison with the cueing mechanism. We also perform ablation studies to observe the contributions of the individual modules. All experiments are conducted on large AVSR data sets consisting of uncontrolled spoken sentences.

A. Dataset

LRS2-BBC [4]: The dataset is an audio-visual collection of more than 143K utterances with a 60K vocabulary from BBC programs. All samples are carefully pre-processed by face detection, shot detection, face tracking, facial landmark detection, audio-visual synchronization, forced audio-subtitle

alignment, and alignment verification. The facial images are captured from both profile and frontal views. The dataset is split into 4 parts: pre-train, train, val, and test. The pre-train set and the train set are for training, while the val set and the test set are for development and test, respectively. The pre-train set comes with a word-level force alignment. The utterances in the other three parts are shorter than 6 seconds, while a small portion of the utterances in the pre-train set are longer than 6 seconds. The training data is around 224 hours.

LRS3-TED [4]: The dataset contains 164K utterances and have a similar vocabulary size to LRS2-BBC, but with longer utterances. The dataset has a total of 438 hours and is split into 3 parts: pre-train, train, and test. The pre-processing of LRS3-TED is the same as that of LRS2-BBC. Like in LRS2-BBC, the pre-train set also comes with word-level force alignment. However, unlike LRS2-BBC, LRS3-TED has no speaker overlap between the training and test sets, because the data of LRS3-TED is from TED videos and is split by presenters.

We choose character-level tokens as ground truth since words in two datasets are unconstrained. There are 40 output classes, namely $C = 40$, including the 26 characters (A-Z), the 10 digits (0-9), the token [space] for separating words, [prime] (′), [sos] indicates the start or end of an utterance, and [blank] for CTC training.

B. Data augmentation

In addition, we inject babble noise into waveforms before STFT and implement a method similar to SpecAugment [55] after STFT to augment the data. In detail, we apply two masks each of which is up to 0.4 seconds on the time axis while we randomly mask two frequency bands where each band is less than 1k Hz. The maximum time warp is 5 frames. We generate the babble noise by mixing samples presented in [4]. During training, we follow the SNR distribution of [17], particularly, an uniform distribution over [No noise, 20dB, 15dB, 10dB, 5dB, 0dB, -5dB].

For video images, patches of 112×112 are horizontally flipped with 50% random selection.

C. Language Model

Following [17], we adopt a transformer-based [56] character-level Language Model (LM). The training corpus has 16.2 million words, which consists of the transcriptions of LibriSpeech (960 hours) [57], pre-train and train sets of LRS2-BBC [4] and LRS3-TED [4]. Each character is encoded to a 128-D vector without positional encoding. d_a and h of the MHSA and d_f of the FFN in transformer blocks are 8, 512 and 2048, respectively. Besides, the LM contains 16 transformer blocks. We train the LM by Adam optimizer [58] for 30 epochs with the val set of LRS2-BBC as the development set, learning rate 10^{-4} , and batch size 32. LM training is implemented by ESPnet [59] with a single GeForce GTX 1080 Ti (11 GB memory).

D. Pre-training

As described in Sec. III-B, we pre-train the predictor via a lipreading task that takes visual frame sequence as input and generates character posteriors. In the predictor, there are 12 Conformer blocks in the visual Conformer encoder, namely $N_p = 12$. The hyperparameters are $d_k = 256$, $d_a = 256$, $d_{ff} = 2048$, $h = 4$. And the kernel size of the depthwise 1D convolutional layers is 31. Besides, for LRS2-BBC, the visual frontend is trained, which is the same as Fig. 3. But for LRS3-TED, due to limited disk storage and lengthy training procedure if we train the frontend simultaneously, we adopt parameters of the visual frontend from [4] and pre-process image sequences to 512-D visual embeddings via the frozen visual frontend. Because of pre-processing, there is no visual data augmentation for LRS3-TED and we just crop central patches of 112×112 to the visual frontend in the pre-processing. This setting is consistent in the following AVSR experiments.

In the update encoder, we adopt the factorized-excitation FFN instead of a standard FFN, as shown in Fig. 3(b). As both share the same architecture, we can pre-train an audio Conformer [17] to initialize the update encoder. The audio Conformer serves as an audio-based ASR model but replaces its input filter-bank features or convolutional features by spectrum from STFT. There are 12 Conformer blocks in the ASR Conformer encoder. The hyper-parameters of the ASR encoder are the same as that of the lipreading encoder except for the attention head $h = 8$.

The pre-trained lipreading and ASR model share the same decoder architecture as that of the P&U net in Sec. III-D, which consists of 6 transformer blocks. The hyper-parameters of MHSA, FFN of the decoder block are set as $d_k = 256$, $d_a = 256$, $d_{ff} = 2048$, $h = 8$.

TABLE I
PERFORMANCE OF VIDEO-ONLY MODEL GIVEN THE METRIC OF CHARACTER ERROR RATE (CER). LM: LANGUAGE MODEL.

Inference Method	CTC	CTC&LM	CTC&Decoder&LM
LRS2-BBC	32.2%	28.8%	27.2%
LRS3-TED	40.1%	36.5%	34.6%

We report the performance of the pre-trained lipreading model in Tab. I. The CTC inference results are solely based on the output of the predictor ρ . The CTC&LM denotes the system that infers a text sequence by incorporating an external language model of characters. The CTC&Decoder&LM system further involves the decoder. When the CTC, the decoder, and the LM are all involved during frame-by-frame inference, the output of LM, the decoder, and the CTC module are summed up with their respective weight of ψ , γ , and $1 - \gamma$ to form a final probability distribution. The top-1 character is used as the output. We empirically set $\gamma = 0.1$, $\psi = 0.6$ for LRS2-BBC. As the LM is optimized on the val set of LRS2-BBC, there could be a mismatch with LRS3-TED. Therefore, we choose $\gamma = 0.2$, $\psi = 0.4$ for LRS3-TED. Moreover, beam search is employed with a width of 20.

It is reported that the CTC inference by the predictor alone achieves a character error rate of 32.2% and 40.1% for top-1 decoding on LRS2-BBC and LRS3-TED datasets. By incorporating the LM and decoder, the lipreading model is further improved. As we use the visual embedding ρ rather than the top-1 decoding as the visual cue, we believe that the lipreading model provides informative visual cues.

E. Implementation details

The predictor and the update encoder are initialized by the parameters of the encoders of the pre-trained lipreading and ASR models, respectively, while the decoder parameters are initialized by the decoder of the lipreading model. For the variant of the visual embedding ρ' , its dimension $K = 32$ because 32 is the closest number to the number of output classes and meanwhile is the divisor of the hidden vector dimension of vanilla FFN d_{ff} . Consequently, the dimension of audio sub-spaces $d_l = 64$.

We implement our models on a single GeForce RTX 3090 (24 GB memory). The network is trained by Adam optimizer [58] with $\beta_1 = 0.9$, $\beta_2 = 0.98$, and $\epsilon = 10^{-9}$. Batch sizes are 8 for LRS2-BBC and 16 for LRS3-TED. Optimizers take a step every 4 and 2 batches for two dataset. The learning rate linearly increases to 2×10^{-4} by 25000 steps and afterwards decreases proportionally to the inverse square root of the step number, which is employed in [39].

For experiments on LRS2-BBC, we mix its pre-train and train sets as the training set and exclude samples with more than 24 seconds. Because the mixed training set contains more than 140K utterances, we process them by virtual epochs, randomly picking 16,384 samples from the mixed set. The network is trained for 500 virtual epochs. And only samples within 6 seconds will be picked at the first 100 epochs, which is similar to curriculum learning [4].

For experiments on LRS3-TED, the virtual epoch, the mixture of pre-train and trainval set, and the curriculum learning are employed as well. The difference is that we only exclude samples of more than 48 seconds, and we train the network for 750 virtual epochs, as LRS3-TED are bigger than LRS2-BBC.

At the inference phase, the attention decoder module, the CTC module and the LM are employed together. We set the same weights as that in IV-D, namely, $\gamma = 0.1$, $\psi = 0.6$ for LRS2-BBC, $\gamma = 0.2$, $\psi = 0.4$ for LRS3-TED.

Besides, we implement the feature concatenation (Feat Concat) as a contrastive model of the P&U net (early4) to show the benefit of cueing mechanism. The Feat Concat fuses audio and visual features described in Sec. III-A by simply joining the time-aligned audio and visual features into a single feature. Before the concatenation, two features are normalized to a similar scale. Subsequently, the concatenated audio-visual feature vector is reduced to a 256-D vector by passing through two linear layers, that is then taken by the 12 Conformer blocks ($d_k = 256$, $d_a = 256$, $d_{ff} = 2048$, $h = 8$). The loss function of the Feat Concat is the same as the P&U net.

F. Cueing at different stage

As shown in Fig. 3(c)-3(d), the order of the cross-modal Conformer blocks and the Conformer block is inter-

changeable. There are a total of 12 blocks in the update encoder. In particular, we design an experiment with five configurations: P&U net (early4) and P&U net (early8) as Fig. 3(c): First 4 and 8 blocks are cross-modal Conformer blocks; P&U net (middle): middle 4 blocks are cross-modal Conformer blocks; P&U net (late) as Fig. 3(d): last 4 blocks are cross-modal Conformer blocks; and P&U net (all): All 12 blocks are cross-modal Conformer blocks. We report the results in the Tab. II, where “clean” and “noisy” denote the original test samples without or with 0 dB babble noise.

TABLE II
PERFORMANCE COMPARISON IN WER OF VISUAL EMBEDDING CUES
DIFFERENT LEVELS OF AUDIO FEATURES WITH EXTERNAL LM. NOISY:
UNDER 0 DB BABLE NOISE.

Dataset	LRS2-BBC		LRS3-TED	
	Clean	Noisy	Clean	Noisy
P&U net (early4)	3.83%	9.50%	3.05%	8.48%
P&U net (middle)	4.11%	11.33%	3.14%	9.69%
P&U net (late)	4.61%	14.23%	3.62%	12.75%
P&U net (early8)	3.71%	9.89%	3.26%	8.51%
P&U net (all)	3.87%	11.62%	3.52%	9.78%

Under the clean condition, the results of LRS2-BBC in Tab. II show that the P&U net (early4) achieves a WER of 3.83%, which outperforms the P&U net (middle), whose WER is 4.11% with a relative WER reduction of 6.8%. The P&U net (late) only achieves a WER of 4.61%, which lags behind the P&U net (middle) by a 10.8% relative WER. These results suggest that fusion at an earlier stage is more effective than fusion at a later stage as far as visual cueing is concerned. The same trend is observed on LRS3-TED. The P&U net (early4), P&U net (middle) and P&U net (late) achieve the WER of 3.05%, 3.14%, and 3.62%.

We use the decoding of an utterance as an example in Tab. III to show how the different systems behave. The visual cue with an early cueing provides an accurate phonetic prediction that cannot be perceived in the audio signal, *i.e.*, the non-audible release of /d/ at the end of “PICKLED”.

TABLE III
AN AVSR EXAMPLE IN THE CLEAN ENVIRONMENT. AUDIO:
PRE-TRAINED ASR MODEL; VIDEO: PRE-TRAINED LIPREADING MODEL;
GT: GROUND TRUTH.

Transcription	
GT	THAT'S A PICKLED WALNUT
P&U net (early4)	THAT'S A PICKLED WALNUT
P&U net (middle)	THAT'S A PICKLE WALNUT
P&U net (late)	THAT TO PICKLE WALNUT
Audio	THAT'S A PICKLE WALNUT
Video	THAT'S THE BUILDING

Under the noisy condition, speech signals are corrupted by babble noise with the resulting SNR of 0 dB. We observe the same performance trend as under the clean condition. On LRS2-BBC, the P&U net (middle) only achieves a WER of 11.33%, which is worse than the P&U net (early4), whose WER is 9.5%, by a relative reduction of 16.2%. The P&U

net (late) obtains a WER of 14.23%, which lags behind the P&U net (middle) by a relative reduction of 20.4%. The results in LRS3-TED are consistent with those in LRS2-BBC. The relative WER reductions from the P&U net (early4) to (middle), and from the P&U net (middle) to (late) are 12.5% (9.69% to 8.48%) and 24% (12.75% to 9.69%), respectively. Moreover, we observe that the performance drops from P&U net (middle) to (late) is greater than that from P&U net (early4) to (middle), *i.e.*, 20.4% vs. 16.2% on LRS2-BBC, and 24% vs. 12.5% on LRS3-TED. All results strongly suggest applying visual cueing at an earlier stage is beneficial.

The results also show that early cueing is more effective in a noisy environment than late cueing. We can observe that the performance drops from P&U net (early4) to (middle) are 6.8% and 16.2% under the clean and noisy conditions on LRS2-BBC, respectively. The same phenomenon exists in such a comparison on LRS3-TED.

TABLE IV

AN EXAMPLE OF AV RESULT IN THE NOISY ENVIRONMENT. AUDIO: PRE-TRAINED ASR MODEL; VIDEO: PRE-TRAINED LIPREADING MODEL; GT: GROUND TRUTH; P&U NET IS OMITTED BEFORE (EARLY4), (MIDDLE) AND (LATE).

Transcription	
GT	INSTEAD OF BEING SOMEONE'S ARM CANDY
Early4	INSTEAD OF BEING SOMEONE'S ARM CANDY
Middle	INSTEAD OF BEING SOMEONE'S FAMILY
Late	INSTEAD OF BEING SOMEONE'S AUNTIE
Audio	INSTEAD OF BEING SOMEONE'S ON KENT
Video	SELF BECAUSE IT WASN'T COMPLICATED

We use the decoding of an utterance as an example in Tab. IV to show how the different systems behave under 0 dB babble noise. The visual cue with an earlier fusion provides an accurate phonetic prediction that differentiates /m/ and /n/ in a better way than the audio cue alone.

In Tab. II, we also observe that the P&U net (early8) hardly outperforms the P&U net (early4). Furthermore, the P&U net (early4) exceeds the P&U net (all) across the board, suggesting that additional later cross-modal cueing is not contributing.

G. Comparative study

We compare the P&U net and other SOTA systems on LRS2-BBC in Tab. V. We observe that the P&U net (early4) significantly outperforms other systems both under clean and noisy conditions. Particularly, let us use the best-performing AV Conformer [17] (fusion of separate audio and visual context representation) as the baseline, which has the same learnable parameter as ours. The P&U net (early4) achieves a relative WER reduction of 16.3%, *i.e.*, from a 4.3% WER to a 3.6% WER, over the baseline under the clean condition. We also observe a 42.0% relative WER reduction, *i.e.*, from a 15.7% WER to a 9.1% WER, under the noisy condition.

To appreciate the contribution of the visual cueing mechanism, we first compare the worst-performing P&U net (late)

*we re-implement the algorithm using inputs, noise, training procedure, LM described in this paper.

TABLE V
COMPARISON OF OUR PROPOSED METHOD WITH SOME SOTA METHODS ON THE LRS2-BBC DATASET. ENTRIES IN COLUMNS OF CLEAN AND NOISY INDICATE WER WITH EXTERNAL LM. NOISY: ORIGINAL WAVEFORM PLUS 0 DB BABBLE NOISE.

Method	Training data	Clean	Noisy
TM-seq2seq[4]	MVLRS(730)+LRS2&3 ^{0.4} (632)	8.5%	34.2%
TM-CTC[4]	MVLRS(730)+LRS2&3 ^{0.4} (632)	8.2%	23.6%
DCM[16]	LRS2(224)	8.6%	28.9%
CTC/Attention[29]	LRW(157)+LRS2(224)	7.0%	-
TDNN[30]	LRS2(224)	5.9%	-
AV Conformer*[17]	LRS2(224)	4.3%	15.7%
Feat Concat	LRS2(224)	4.4%	11.5%
P&U net (late)	LRS2(224)	4.6%	14.2%
P&U net (early4)	LRS2(224)	3.6%	9.1%

and the baseline. The P&U net (late) conducts audio-visual fusion after audio features have passed through 8 Conformer blocks and its performance with clean utterance is worse than that of the baseline (4.6% vs. 4.3%). But the P&U net (late) still outperforms the baseline by a 9.6% relative WER (14.2% vs. 15.7%) in the noisy environment, as shown in Tab. V. We are convinced that the visual cueing mechanism contributes to the performance gain by P&U net under the noisy condition.

We also compare the P&U net (early4) and the Feat Concat. Both of them adopt an early fusion strategy, but differ in how audio-visual signals are fused, as discussed in Sec. III-E. As shown in Tab. V, the P&U net (early4) outperforms the Feat Concat under both clean (3.6% WER vs. 4.4% WER) and noisy condition (9.1% WER vs. 11.5% WER) by approximately 20% relative WER reduction. We attribute the performance gain to the visual cueing mechanism.

We further compare the systems on LRS3-TED in Tab. VI. We observe that the P&U net (early4) outperforms other SOTA methods, especially under the noisy condition. In particular, the P&U net (early4) leads AV Conformer by 10% relative WER (3.0% vs. 3.3%) and 42.4% relative WER (8.3% vs. 14.4%) under the clean and noisy condition, respectively. Besides, the P&U net (early4) also outperforms Feat Concat under both the clean and noisy conditions, which confirms the benefit of cueing mechanism again.

TABLE VI
COMPARISON OF OUR PROPOSED METHOD WITH SOME STATE-OF-THE-ART METHODS ON THE LRS3-TED. ENTRIES IN CLEAN AND NOISY COLUMNS INDICATE WER WITH EXTERNAL LM. NOISY: ORIGINAL WAVEFORM PLUS 0 DB BABBLE NOISE.

Method	Training data	Clean	Noisy
TM-seq2seq[4]	MVLRS(730)+LRS2&3 ^{0.4} (632)	7.2%	42.5%
TM-CTC[4]	MVLRS(730)+LRS2&3 ^{0.4} (632)	7.5%	27.7%
DCM[16]	LRS3 ^{0.4} (438)	8.8%	30.9%
EG-s2s[35]	LRS3 ^{0.0} (474)	6.8%	25.5%
RNN-T[13]	YT(31k)	4.5%	-
Attentive Fusion[60]	LRS3 ^{0.4} (438)	6.4%	-
AV Conformer*[17]	LRS3 ^{0.4} (438)	3.3%	14.4%
Feat Concat	LRS3 ^{0.4} (438)	3.3%	10.1%
P&U net (late)	LRS3 ^{0.4} (438)	3.6%	12.8%
P&U net (early4)	LRS3 ^{0.4} (438)	3.0%	8.3%

H. Visual cueing vs. context representation concatenation

To appreciate how the visual cueing mechanism works under noisy condition, we compare the audio-visual context representation R , i.e. the output of the update encoder in the P&U net (late), and the fusion of audio and visual context representations in the baseline. We measure the cosine similarity as expressed in Eq. 7 between the audio-visual context representations R for speech signals without noise and R' for that with different SNR noise.

$$\theta_t^j = \frac{R_t^j \cdot R'_t{}^j}{\|R_t^j\| \cdot \|R'_t{}^j\|} \quad (7)$$

where j and t indicate an utterance index and a frame index, respectively. $\theta \in [-1, 1]$ denotes the cosine similarity.

We report the average cosine similarities of the two networks across all time frames and utterances on the LRS2-BBC test set in the Tab. VII. The cosine similarity θ of both networks approaches 1.0 when $\text{SNR} \geq 15$ dB. We also observe that the cosine similarity of the P&U net (late) is consistently higher than that of the baseline. As the SNR decreases, θ of the baseline deteriorates rapidly, while θ of the P&U net (late) remains steady. The results in Tab. VII account for why the P&U net (late) performs worse than the baseline under the clean condition but otherwise under 0 dB SNR, which shows the benefit of the visual cueing mechanism under the noisy condition.

TABLE VII

THE COSINE SIMILARITY BETWEEN THE AUDIO-VISUAL CONTEXT REPRESENTATIONS R AND R' FOR SPEECH SIGNALS AT DIFFERENT SNR ON THE LRS2-BBC DATASET.

Methods	20 dB	15 dB	10 dB	5 dB	0 dB	-5 dB
P&U net (late)	0.994	0.987	0.973	0.949	0.919	0.923
AV Conformer*[17]	0.987	0.972	0.94.5	0.885	0.778	0.721

I. Initialization by pre-trained models

The P&U net benefits from the pre-trained ASR and lipreading models as described in Sec. IV-D. Fig. 5 shows the WER as a function of the number of training epochs for the P&U net and the baseline AV Conformer. The P&U nets are initialized by the pre-trained unimodal models. We also compare AV Conformer with random initialization as a contrast. We can see that the AV Conformer converges more quickly with the pre-trained models than without.

J. Dimension of visual embedding

We are interested in the effect of the pre-defined parameters of the factorized-excitation FFN, for example, the number of audio feature subspaces K , which also determines the dimension of audio feature sub-spaces d_l . To this end, we design an experiment on LRS2-BBC and LRS3-TED with four different $K=16, 32, 64, 128$, thus, $d_l=128, 64, 32, 16$ with the P&U net (early4), and report the WER results in Tab. VIII.

It is observed that the dimension K does not significantly affect the results under both clean and noisy conditions and

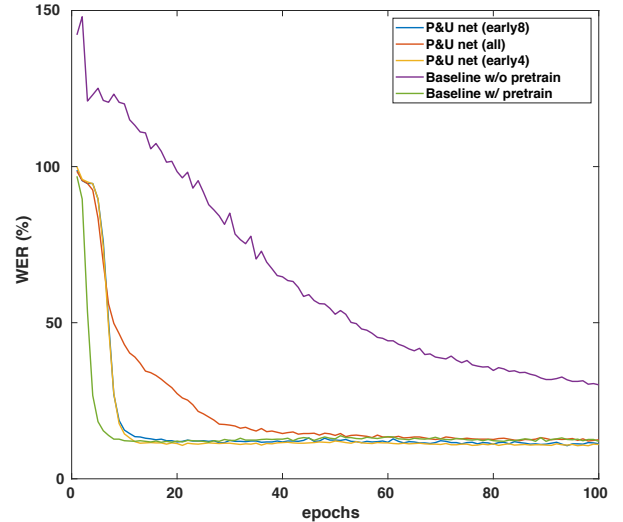


Fig. 5. The WER training curves on LRS2-BBC val set in a teacher forcing mode.

TABLE VIII

EXPERIMENTS ON THE VISUAL EMBEDDING, i.e., CHARACTER POSTERIORS, FOR CLEAN SPEECH SIGNALS AND NOISY SPEECH SIGNALS CORRUPTED BY 0 dB BABBLE NOISE.

Dataset	LRS2-BBC		LRS3-TED	
Dimension	Clean	Noisy	Clean	Noisy
K=16	3.63%	9.13%	3.02%	8.25%
K=32	3.83%	9.50%	3.05%	8.48%
K=64	3.67%	9.97%	3.07%	8.15%
K=128	3.62%	9.16%	3.01%	8.38%

in both LRS2-BBC and LRS3-TED datasets. Therefore, in the rest of the experiments, we have chosen $K=32$.

K. Position of the factorized-excitation FFN

We design the cross-modal Conformer block by replacing an FFN module with a factorized-excitation FFN. As shown in Fig. 3(a), there are two FFN modules in a Conformer block. We alter the position of the factorized-excitation FFN by 1) replacing the first FFN module, 2) replacing the second FFN module and 3) replacing both FFN modules. All three configurations are implemented on the P&U net (early4) with the audio subspace dimension $d_l = 64$.

TABLE IX

EXPERIMENTS ON THE POSITION OF THE FACTORIZED-EXCITATION (FE) FFN FOR CLEAN SPEECH SIGNALS AND NOISY SPEECH SIGNALS CORRUPTED BY 0 dB BABBLE NOISE.

Position of FE FFN	Clean	Noisy
first FFN	3.66%	9.28%
second FFN	3.83%	9.50%
both FFN	4.25%	10.86%

As in Tab. IX we observe that replacing the first FFN performs slightly better than the second one, which confirms the benefit of early cueing. Replacing both FFN does not

achieve performance gain suggests that visual cue plays a secondary role in the audio-visual speech recognition.

V. CONCLUSION

We have proposed a novel end-to-end audio-visual speech recognition network architecture, *i.e.*, the P&U net. This study is motivated by the finding in human speech perception where visual signals prime the listener before the arrival of audio signals. We hypothesize that the visual cueing mechanism and early fusion are the two contributing factors to effective audio-visual speech recognition. The experiments have validated our hypotheses. The fact that the visual cueing mechanism has a clear advantage over the simple fusion suggests that the interaction between audio and visual signals is as important as the signals themselves as far as speech recognition is concerned.

REFERENCES

- [1] Z. Pan, R. Tao, C. Xu, and H. Li, "Selective listening by synchronizing speech with lips," *IEEE/ACM Trans. on Audio, Speech and Language Processing*, 2022.
- [2] R. Tao, Z. Pan, R. K. Das, X. Qian, M. Z. Shou, and H. Li, "Is someone speaking? exploring long-term temporal features for audio-visual active speaker detection," in *Proc. of ACM Int. Conf. on Multimedia*, 2021, pp. 3927–3935.
- [3] Y. Kim, H. Lee, and E. M. Provost, "Deep learning for robust feature generation in audiovisual emotion recognition," in *Proc. of IEEE Int. Conf. on Audio, Speech and Signal Processing*, 2013, pp. 3687–3691.
- [4] T. Afouras, J. S. Chung, A. Senior, O. Vinyals, and A. Zisserman, "Deep audio-visual speech recognition," *IEEE Trans. on Pattern Analysis and Machine Intelligence*, 2018.
- [5] I. C. Yadav and G. Pradhan, "Pitch and noise normalized acoustic feature for children's asr," *Digital Signal Processing*, vol. 109, p. 102922, 2021.
- [6] D. W. Massaro and D. G. Stork, "Speech recognition and sensory integration: a 240-year-old theorem helps explain how people and machines can integrate auditory and visual information to understand speech," *American Scientist*, vol. 86, no. 3, pp. 236–244, 1998.
- [7] L. Cappelletta and N. Harte, "Phoneme-to-viseme mapping for visual speech recognition," in *Proc. of Int. Conf. on Pattern Recognition Applications and Methods*, 2012, pp. 322–329.
- [8] Q. Summerfield, "Some preliminaries to comprehensive account of audio-visual speech perception," *Hearing by Eye: the Psychology of Lipreading*, vol. 3, pp. 746–748, 1976.
- [9] J. Luettin, G. Potamianos, and C. Neti, "Asynchronous stream modeling for large vocabulary audio-visual speech recognition," in *Proc. of IEEE Int. Conf. on Audio, Speech and Signal Processing*, vol. 1, 2001, pp. 169–172.
- [10] D. Stewart, R. Seymour, A. Pass, and J. Ming, "Robust audio-visual speech recognition under noisy audio-video conditions," *IEEE Trans. on Cybernetics*, vol. 44, no. 2, pp. 175–184, 2013.
- [11] W. Yu, S. Zeiler, and D. Kolossa, "Fusing information streams in end-to-end audio-visual speech recognition," in *Proc. of IEEE Int. Conf. on Audio, Speech and Signal Processing*, 2021, pp. 3430–3434.
- [12] D. Serdyuk, O. Braga, and O. Siohan, "Transformer-based video front-ends for audio-visual speech recognition," *arXiv preprint arXiv:2201.10439*, 2022.
- [13] T. Makino, H. Liao, Y. Assael, B. Shillingford, B. Garcia, O. Braga, and O. Siohan, "Recurrent neural network transducer for audio-visual speech recognition," in *Proc. of IEEE Workshop on Automatic Speech Recognition and Understanding*, 2019, pp. 905–912.
- [14] B. Shi, W.-N. Hsu, K. Lakhotia, and A. Mohamed, "Learning audio-visual speech representation by masked multimodal cluster prediction," *arXiv preprint arXiv:2201.02184*, 2022.
- [15] G. Sterpu, C. Saam, and N. Harte, "How to teach dnns to pay attention to the visual modality in speech recognition," *IEEE/ACM Trans. on Audio, Speech and Language Processing*, vol. 28, pp. 1052–1064, 2020.
- [16] Y.-H. Lee, D.-W. Jang, J.-B. Kim, R.-H. Park, and H.-M. Park, "Audio-visual speech recognition based on dual cross-modality attentions with the transformer model," *Applied Sciences*, vol. 10, no. 20, p. 7263, 2020.
- [17] P. Ma, S. Petridis, and M. Pantic, "End-to-end audio-visual speech recognition with conformers," in *Proc. of IEEE Int. Conf. on Audio, Speech and Signal Processing*, 2021, pp. 7613–7617.
- [18] E. Z. Golumbic, G. B. Cogan, C. E. Schroeder, and D. Poeppel, "Visual input enhances selective speech envelope tracking in auditory cortex at a "cocktail party"," *Journal of Neuroscience*, vol. 33, no. 4, pp. 1417–1426, 2013.
- [19] K. W. Grant and P.-F. Seitz, "The use of visible speech cues for improving auditory detection of spoken sentences," *The Journal of the Acoustical Society of America*, vol. 108, no. 3, pp. 1197–1208, 2000.
- [20] K. W. Grant, "The effect of speechreading on masked detection thresholds for filtered speech," *The Journal of the Acoustical Society of America*, vol. 109, no. 5, pp. 2272–2275, 2001.
- [21] D. Byrd, "54,000 american stops," *UCLA working Papers in Phonetics*, vol. 83, pp. 97–116, 1993.
- [22] J.-L. Schwartz, F. Berthommier, and C. Savariaux, "Seeing to hear better: evidence for early audio-visual interactions in speech identification," *Cognition*, vol. 93, no. 2, pp. B69–B78, 2004.
- [23] L. A. Varghese, E. J. Ozmeral, V. Best, and B. G. Shinn-Cunningham, "How visual cues for when to listen aid selective auditory attention," *Journal of the Association for Research in Otolaryngology*, vol. 13, no. 3, pp. 359–368, 2012.
- [24] A. Doucet, S. Godsill, and C. Andrieu, "On sequential monte carlo sampling methods for bayesian filtering," *Statistics and computing*, vol. 10, no. 3, pp. 197–208, 2000.
- [25] R. E. Kalman, "A new approach to linear filtering and prediction problems," 1960.
- [26] A. H. Abdelaziz, S. Zeiler, and D. Kolossa, "Learning dynamic stream weights for coupled-hmm-based audio-visual speech recognition," *IEEE/ACM Trans. on Audio, Speech and Language Processing*, vol. 23, no. 5, pp. 863–876, 2015.
- [27] H. Meutzner, N. Ma, R. Nickel, C. Schymura, and D. Kolossa, "Improving audio-visual speech recognition using deep neural networks with dynamic stream reliability estimates," in *Proc. of IEEE Int. Conf. on Audio, Speech and Signal Processing*, 2017, pp. 5320–5324.
- [28] A. K. Katsaggelos, S. Bahaadini, and R. Molina, "Audiovisual fusion: Challenges and new approaches," *Proceedings of the IEEE*, vol. 103, no. 9, pp. 1635–1653, 2015.
- [29] S. Petridis, T. Stafylakis, P. Ma, G. Tzimiropoulos, and M. Pantic, "Audio-visual speech recognition with a hybrid ctc/attention architecture," in *IEEE Spoken Language Technology Workshop*, 2018, pp. 513–520.
- [30] J. Yu, S.-X. Zhang, J. Wu, S. Ghorbani, B. Wu, S. Kang, S. Liu, X. Liu, H. Meng, and D. Yu, "Audio-visual recognition of overlapped speech for the Irs2 dataset," in *Proc. of IEEE Int. Conf. on Audio, Speech and Signal Processing*, 2020, pp. 6984–6988.
- [31] H. Liu, W. Xu, and B. Yang, "Audio-visual speech recognition using a two-step feature fusion strategy," in *Proc. of Int. Conf. on Pattern Recognition*, 2021, pp. 1896–1903.
- [32] D. Hu, C. Wang, F. Nie, and X. Li, "Dense multimodal fusion for hierarchically joint representation," in *Proc. of IEEE Int. Conf. on Audio, Speech and Signal Processing*, 2019, pp. 3941–3945.
- [33] G. Paraskevopoulos, S. Parthasarathy, A. Khare, and S. Sundaram, "Multiresolution and multimodal speech recognition with transformers," *arXiv preprint arXiv:2004.14840*, 2020.
- [34] J. Ngiam, A. Khosla, M. Kim, J. Nam, H. Lee, and A. Y. Ng, "Multimodal deep learning," in *Proc. of Int. Conf. on Machine Learning*, 2011.
- [35] B. Xu, C. Lu, Y. Guo, and J. Wang, "Discriminative multi-modality speech recognition," in *Proc. of Int. Conf. on Computer Vision and Pattern Recognition*, 2020, pp. 14 433–14 442.
- [36] K. He, X. Zhang, S. Ren, and J. Sun, "Deep residual learning for image recognition," in *Proc. of Int. Conf. on Computer Vision and Pattern Recognition*, 2016, pp. 770–778.
- [37] S. Hochreiter and J. Schmidhuber, "Long short-term memory," *Neural computation*, vol. 9, no. 8, pp. 1735–1780, 1997.
- [38] K. Cho, B. Van Merriënboer, C. Gulcehre, D. Bahdanau, F. Bougares, H. Schwenk, and Y. Bengio, "Learning phrase representations using rnn encoder-decoder for statistical machine translation," *arXiv preprint arXiv:1406.1078*, 2014.
- [39] A. Vaswani, N. Shazeer, N. Parmar, J. Uszkoreit, L. Jones, A. N. Gomez, Ł. Kaiser, and I. Polosukhin, "Attention is all you need," *Advances in Neural Information Processing Systems*, vol. 30, 2017.
- [40] X. Zhang, F. Cheng, and S. Wang, "Spatio-temporal fusion based convolutional sequence learning for lip reading," in *Proc. of Int. Conf. on Computer Vision and Pattern Recognition*, 2019, pp. 713–722.

- [41] J. Li, V. Lavrukhin, B. Ginsburg, R. Leary, O. Kuchaiev, J. M. Cohen, H. Nguyen, and R. T. Gadde, “Jasper: An end-to-end convolutional neural acoustic model,” *Proc. of International Speech Communication Association*, pp. 71–75, 2019.
- [42] T. Afouras, J. S. Chung, and A. Zisserman, “Asr is all you need: Cross-modal distillation for lip reading,” in *ICASSP, pages=2143–2147, year=2020*.
- [43] A. Gulati, J. Qin, C.-C. Chiu, N. Parmar, Y. Zhang, J. Yu, W. Han, S. Wang, Z. Zhang, Y. Wu *et al.*, “Conformer: Convolution-augmented transformer for speech recognition,” *arXiv preprint arXiv:2005.08100*, 2020.
- [44] M. Delcroix, K. Kinoshita, T. Hori, and T. Nakatani, “Context adaptive deep neural networks for fast acoustic model adaptation,” in *Proc. of IEEE Int. Conf. on Audio, Speech and Signal Processing*, 2015, pp. 4535–4539.
- [45] K. Žmolíková, M. Delcroix, K. Kinoshita, T. Ochiai, T. Nakatani, L. Burget, and J. Černocký, “Speakerbeam: Speaker aware neural network for target speaker extraction in speech mixtures,” *IEEE Journal of Selected Topics in Signal Processing*, vol. 13, no. 4, pp. 800–814, 2019.
- [46] N. Dehak, P. J. Kenny, R. Dehak, P. Dumouchel, and P. Ouellet, “Front-end factor analysis for speaker verification,” *IEEE/ACM Trans. on Audio, Speech and Language Processing*, vol. 19, no. 4, pp. 788–798, 2010.
- [47] R. Gu, S.-X. Zhang, Y. Xu, L. Chen, Y. Zou, and D. Yu, “Multi-modal multi-channel target speech separation,” *IEEE Journal of Selected Topics in Signal Processing*, vol. 14, no. 3, pp. 530–541, 2020.
- [48] H. R. V. Joze, A. Shaban, M. L. Iuzzolino, and K. Koishida, “Mmtm: Multimodal transfer module for cnn fusion,” in *Proc. of Int. Conf. on Computer Vision and Pattern Recognition*, 2020, pp. 13 289–13 299.
- [49] P. Ma, S. Petridis, and M. Pantic, “Investigating the lombard effect influence on end-to-end audio-visual speech recognition,” *Proc. of International Speech Communication Association*, pp. 4090–4094, 2019.
- [50] A. Graves, S. Fernández, F. Gomez, and J. Schmidhuber, “Connectionist temporal classification: labelling unsegmented sequence data with recurrent neural networks,” in *Proc. of Int. Conf. on Machine Learning*, 2006, pp. 369–376.
- [51] S. Watanabe, T. Hori, S. Kim, J. R. Hershey, and T. Hayashi, “Hybrid ctc/attention architecture for end-to-end speech recognition,” *IEEE Journal of Selected Topics in Signal Processing*, vol. 11, no. 8, pp. 1240–1253, 2017.
- [52] J. Son Chung, A. Senior, O. Vinyals, and A. Zisserman, “Lip reading sentences in the wild,” in *Proc. of Int. Conf. on Computer Vision and Pattern Recognition*, 2017, pp. 6447–6456.
- [53] X. Gao, C. Gupta, and H. Li, “Automatic lyrics transcription of polyphonic music with lyrics-chord multi-task learning,” *IEEE/ACM Trans. on Audio, Speech and Language Processing*, vol. 30, pp. 2280–2294, 2022.
- [54] ———, “Genre-conditioned acoustic models for automatic lyrics transcription of polyphonic music,” in *Proc. of IEEE Int. Conf. on Audio, Speech and Signal Processing*, 2022, pp. 791–795.
- [55] D. S. Park, W. Chan, Y. Zhang, C.-C. Chiu, B. Zoph, E. D. Cubuk, and Q. V. Le, “SpecAugment: A simple data augmentation method for automatic speech recognition,” *arXiv preprint arXiv:1904.08779*, 2019.
- [56] K. Irie, A. Zeyer, R. Schlüter, and H. Ney, “Language modeling with deep transformers,” *arXiv preprint arXiv:1905.04226*, 2019.
- [57] V. Panayotov, G. Chen, D. Povey, and S. Khudanpur, “Librispeech: an asr corpus based on public domain audio books,” in *Proc. of IEEE Int. Conf. on Audio, Speech and Signal Processing*, 2015, pp. 5206–5210.
- [58] D. P. Kingma and J. Ba, “Adam: A method for stochastic optimization,” *arXiv preprint arXiv:1412.6980*, 2014.
- [59] S. Watanabe, T. Hori, S. Karita, T. Hayashi, J. Nishitoba, Y. Unno, N. E. Y. Soplin, J. Heymann, M. Wiesner, N. Chen *et al.*, “Espnet: End-to-end speech processing toolkit,” *arXiv preprint arXiv:1804.00015*, 2018.
- [60] L. Wei, J. Zhang, J. Hou, and L. Dai, “Attentive fusion enhanced audio-visual encoding for transformer based robust speech recognition,” in *Proc. of Asia-Pacific Signal and Information Processing Association Annual Summit and Conf.*, 2020, pp. 638–643.